Journal of Hospital Infection 170 (2026) 236–245

Available online at www.sciencedirect.com

Journal of Hospital Infection

journal homepage: www.elsevier.com/locate/jhin

Source control with masks and respirators in hospitals: exhalation aerosol shedding, jet suppression, and near-/far-field persistence

W. Yang [a,b,*], W.R. Myers [b], K.J. Ryan [c], L. Zheng [a], Y. Zhang [a], X. Li [a]

[a] *School of Safety Engineering, China University of Mining and Technology, Xuzhou, Jiangsu, China*
[b] *Department of Industrial and Management Systems Engineering, Statler College of Engineering and Mineral Resources, West Virginia University, Morgantown, WV, USA*
[c] *Department of Statistics, West Virginia University, Morgantown, WV, USA*

ARTICLE INFO

Article history:
Received 27 October 2025
Accepted 31 January 2026
Available online 14 February 2026

Keywords:
Source control
Elastomeric half-mask respirator (EHMR)
N95 filtering facepiece respirator
Surgical mask
Near-field
Far-field
Total outward leakage (TOL)
Ventilation

SUMMARY

Background: Infectious exhalation aerosol source control using masks and respirators in hospitals depends on the aerosol shedding and its dispersion.
Methods: In a simulation study with a headform, we used a leakage testing system for total outward leakage (TOL) and count median diameter (CMD) and a separate hood for horizontal exhalation-jet velocity at 1, 2, and 3 ft (0.30, 0.61, 0.91 m). Neutralised NaCl aerosols were generated to mimic human exhalation shedding. Five devices for source control – surgical mask (SM), non-valved N95 filtering facepiece respirator (N95 FFR), valved N95 (FFRV), elastomeric half-mask respirator (EHMR), and EHMR with an SM overlay (EHMRSM) – were tested under three faceseal conditions (0%, 50%, and 100%) and three flow rates (17, 28, 39 L min^{-1}). We derived a near-field (NF) emission index and a far-field (FF) persistence index.
Results: Device type significantly affected TOL and CMD ($P < 0.01$). The N95 FFR minimised TOL (≈5–9%) and eliminated horizontal jets, yielding near-zero NF and the lowest FF. The EHMR had the highest TOL (≈82–88%) and persistent jets, producing the largest NF and FF; FFRV was intermediate. The SM and EHMRSM collapsed jets (NF≈0) but retained moderate to high TOL, sustaining elevated FF. Leaked particles were predominantly submicron (CMD ≈ 0.42–0.61 μm).
Conclusions: Gravitational loss (≈0.02–0.05 h^{-1}) is negligible compared with clinical ventilation to clean leaked aerosols, yielding orders of magnitude longer clearance times, so settling alone cannot deliver timely clearance. In practice, low-leakage devices – preferably non-valved N95s – should be paired with adequate air-change rates.

Introduction

Airborne transmission is a major pathway for respiratory infection in hospitals [1–4]. Virus-laden aerosols from human respiration are numerically dominated by fine particles, with

* Corresponding author. Address: No.1, Daxue Road, Xuzhou, Jiangsu, 221116, China, Tel.: +86 18807095192.
E-mail address: weihua.yang@cumt.edu.cn (W. Yang).

https://doi.org/10.1016/j.jhin.2026.01.024
0195-6701/

hospital and indoor studies reporting severe acute respiratory syndrome coronavirus-2 (SARS-CoV-2) RNA peaking at ~0.25–1 μm and often showing a secondary supermicron mode, while classical exhalation work shows abundant production below ~0.8 μm with a substantial fraction <5 μm [5–9].

In mechanically ventilated rooms, submicron aerosols disperse widely and are well described by a first-order, well-mixed balance in which far-field (FF) (room-average) concentrations reflect the source strength and total removal via ventilation, filtration, deposition, and inactivation [10,11]. By contrast, near-field (NF) exposure within roughly one metre additionally depends on the momentum and structure of the exhaled jet [12–14]. From Wells–Riley to World Health Organization (WHO) guidance, the consistent message is that ventilation and filtration set the clearance time scale, whereas the emission rate governs steady-state burden [15–17].

Ventilation targets in healthcare settings are expressed as air changes per hour (ACH) [18]. Airborne infection isolation rooms (AIIRs) and operating theatres are designed for high removal rates; guidance typically specifies ~6–12 ACH for patient rooms and AIIRs and ~20 ACH for operating theatres, with clearance tables linking ACH to 99–99.9% removal times [19]. These benchmarks underpin infection-control practice and connect laboratory measurements to building-scale exposure management [18].

Masks and respirators remain essential for source control, reducing emissions of virus-laden aerosols from infected individuals [20]. Non-valved N95 filtering facepiece respirators (N95 FFRs) are recommended when both protection and source control are required in hospitals [21,22]. Devices with unfiltered exhalation valves (valved N95s, N95 filtering facepiece respirator valved [FFRVs]; elastomeric half-mask respirators [EHMRs]) can leak aerosol outward; guidance discourages their use or requires add-on filtration coverings [23,24].

Visualisations and measurements consistently showed non-valved devices suppress jets and reduce emissions, though gap leakage persists; total outward leakage (TOL) and collection efficiency (CE) were introduced to quantify source control performance [25–31]. The expanded clinical use of EHMRs has prompted evaluation of overlays (surgical mask [SM]) and filtered valves, yet quantitative links from leakage (magnitude and size) and jet behaviour to room-scale risk remain limited [24,32–35].

To address that gap, we employed controlled chambers to measure TOL, the count median diameter (CMD) of leaked aerosol, and horizontal exhalation velocity at 1–3 ft for five types of devices for source control: SMs, N95 FFRs, N95 FFRVs, EHMRs, and EHMRs with an SM overlay on the valve (EHMRSMs). We translated CMD to slip-corrected relaxation/settling parameters, showing gravitational removal of submicron leakage is negligible at clinical ACH and embedded TOL in a well-mixed model to map device emissions to room-average burden [36]. We introduced NF and FF indices to pair leakage with jet momentum and total removal, providing actionable guidance for choosing masks/respirators and setting ventilation targets.

Methods

Tested devices and headforms

Five device types were evaluated for source control, each with two commercial models: SM (Cardinal Health; Aleen), non-valved N95 FFR (3M Aura 9205; Fangtian N058), N95 FFRV (3M Aura 9211; 3M 8511), EHMR (MSA 200LS; 3M 7503), and EHMRSM (same EHMRs with an external Cardinal Health SM overlay). For EHMRSM, an SM was centred over the valve housing; straps were routed around the EHMR head harness; the mask body was positioned flush with the facepiece; and the nose clip was formed to match the EHMR profile. The same procedure was followed for each donning. Figure S1 in the Supplementary Material illustrates how the SM was mounted over the valve of an EHMR. All devices were donned on a single medium-sized ISO standard hard-surface headform. Before data collection for each trial, we conducted a fit test using a PortaCount® Pro+ Respirator Fit Tester (Model 8038, TSI Inc., MN, USA) appropriate to the assigned faceseal condition to verify seal status and repeatability. The overall fit factor of each device under different sealing levels is listed in Table S1 of the Supplementary Material.

Experimental system

Figure 1 shows the TOL testing set-up. Sodium chloride (NaCl) aerosol was generated in a closed conditioning chamber (internal volume $V_{cond} = 1.73\ m^3$; 1.2 m × 1.2 m × 1.2 m) using a particle generator (Model 8026; TSI Inc., Shoreview, MN, USA) and then passed through an electrostatic neutraliser (Model: 3054; TSI, Inc., Shoreview, MN, USA) to approximate Boltzmann charge equilibrium. Temperature and humidity were controlled to 32.2 ± 1.2 °C (90 ± 2 °F) and 60 ± 2% relative humidity using a heater and humidifier, with four mixing fans to promote uniformity.

An upstream three-way valve routed flow to the headform wearing the candidate device inside the TOL test chamber (internal volume $V_{TOL} = 0.26\ m^3$; 0.75 m × 0.59 m × 0.59 m). A breathing simulator with an expandable bladder (Model 1101; Hans Rudolph, Shawnee, KS) provided cyclic inhalation from the generating chamber and exhalation into the TOL chamber. Mask and respirator internal pressure was monitored with a digital gauge (Model AirPro AP800; TSI Inc., Shoreview, MN, USA). Between trials, the chamber was cleared to baseline using a vacuum/high efficiency particulate air conditioning unit. Aerosol was sampled inside and outside the device through fixed ports connected via conductive tubing to an optical particle sizer (OPS; Model 3330; TSI Inc., Shoreview, MN, USA) covering 0.3–10 μm. Tubing runs were kept short and straight to minimise transport losses.

As shown in Figure S2 (Supplementary material), the sampling port inside the mask or respirator was implemented via a copper conduit passing through the headform from back to front, parallel to the breathing line. The inlet of the conduit was beneath the nares at the midline, opened directly into the mask cavity, and was kept flush with the facial plane to avoid disturbing the flow. The outlet terminated at the rear of the headform, where tubing connected to the OPS 3330. This

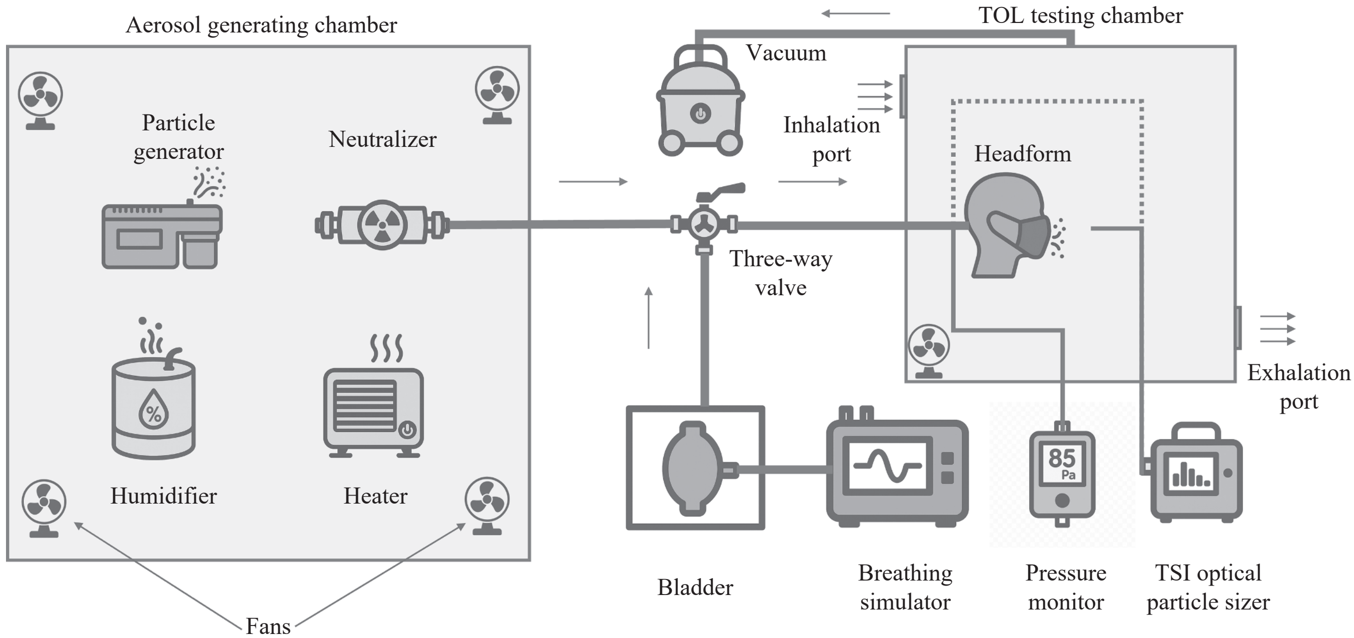

Figure 1. Experimental system for total outward leakage (TOL) testing.

inline, through-headform configuration avoided penetrating the mask shell and standardised the inside sampling location across devices. The sampling port outside the mask or respirator was set in front of the headform and connected to the OPS 3330 through a tube.

Figure 2 depicts the jet-velocity measurement in a hood (1.05 m^3; 1.50 $\times$ 0.70 $\times$ 1.00 m) isolated from building ventilation; the flap could be closed to limit background currents. Peak horizontal exhalation velocity along the jet centreline was measured at 1, 2, and 3 ft (0.30, 0.61, 0.91 m) using calibrated thermal anemometers (Model 9535; TSI Inc.). Background air speeds with the headform idle were $\leq$ 1 cm s^{-1}.

The breathing simulator delivered three mean minute-ventilation levels (17, 28, 39 L min^{-1}) for normal breathing using a sinusoidal waveform with respiratory rates of 20, 25, and 30 breaths·min^{-1} and tidal volumes of 0.85, 1.12, and 1.30 L per breath, respectively, corresponding to light, moderate, and heavy work rates. The minute ventilation flow rates were derived from the body parameters (weight and height) of human subjects reported by Zhu *et al.*, following 'ISO/TS 16976-1' [37,38].

Testing procedure

For each trial, the assigned device was donned under one of three faceseal conditions (Figure S3 of Supplementary Material): 0% (no added seal), 50% (half-perimeter sealing on one side only, left or right randomised by trial, extending continuously from the nasal bridge along the cheek to the chin), and 100% (continuous full-perimeter sealing around the mask edge). For each faceseal condition, inside and outside concentrations were measured at the three flow rates to compute TOL. The OPS logged number concentrations at inside ports for 6 min and then at outside ports for 18 min. Immediately after TOL measurement, the headform (without re-donning) was transferred to the hood for jet testing. At each distance (1, 2, 3 ft), the jet centreline was located and velocity logged at 0.2 Hz for 5 min.

Outcomes

The TOL was defined as the fraction of exhaled aerosol detected outside relative to inside, integrating OPS number concentrations over 0.30—10 μm during exhalation:

$$TOL = \frac{C_{out} - C_{bg}}{C_{in}} \tag{1}$$

where C_{in} and C_{out} are the inside and outside number concentrations, respectively, and C_{bg} is the baseline outside background. The CMD was computed as the 50th percentile of the cumulative number distribution over 0.3—10 μm. NF transport was characterised by the peak horizontal exhalation velocity at 1, 2, and 3 ft (denoted as v_{1ft}, v_{2ftt}, v_{3ft}).

Aerosol-dynamic calculations

For each device-flow condition, the CMD was used as the representative diameter d_p to compute the slip-corrected Stokes relaxation time τ and the terminal settling velocity v_s:

$$\tau(d_p) = \frac{\rho_p {d_p}^2 C_s(d_p)}{18\mu}, v_s(d_p) = g\tau(d_p) \tag{2}$$

where ρ_p is particle density (assumed 1000 kg m^{-3} for exhaled aerosols), μ is the dynamic viscosity of air, g is gravitational acceleration, and C_s is the slip-correction factor:

$$C_s(d_p) = 1 + \frac{\lambda}{d_p}\left(2.34 + 1.05e^{-0.39\frac{d_p}{\lambda}}\right) \tag{3}$$

where λ is the mean free path of air. A notional suspension time over a 1.5-m fall height was $= H/v_s$. Room-average removal was framed with a first-order well-mixed model,

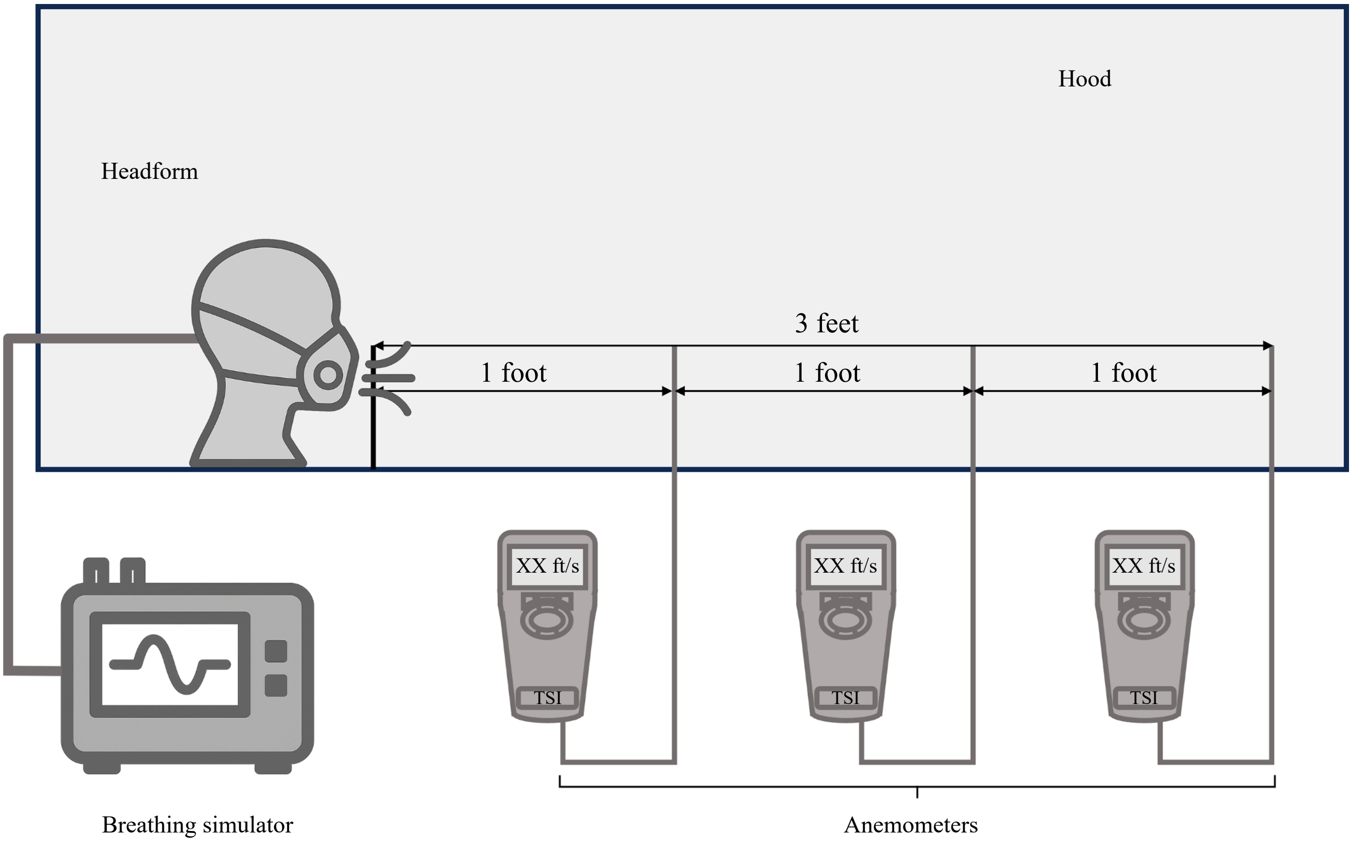

Figure 2. Test set-up to measure the horizontal velocity of exhalation from the headform with and without wearing a surgical mask or respirator.

$$C(t) = C_0 e^{-\Lambda t} \tag{4}$$

where the total first-order loss rate Λ (h^{-1}) is the sum of ventilation (ACH_{vent}), filtration (ACH_{filter}), and gravitational deposition (ACH_{grav}):

$$\Lambda = ACH_{vent} + ACH_{filter} + ACH_{grav} = \frac{Q_{vent}}{V} + \frac{CADR}{V} + \frac{v_s}{H} \times 3600 \tag{5}$$

where Q_{vent} ($m^3 \cdot h^{-1}$) is the supply/exhaust volumetric flow from the heating, ventilation, and air conditioning system and V (m^3) is the room volume; Q_{vent}/V is the ACH from mechanical ventilation. CADR ($m^3 \cdot h^{-1}$) is the clean-air delivery rate from recirculated filtration, so CADR / V is its first-order removal contribution. v_s is the slip-corrected settling velocity derived from the CMD (Eq. 2), and H (m) is the characteristic room height. The factor of 3600 converts s^{-1} to h^{-1} so that all three terms share units of h^{-1}.

Well-mixed clearance model and practical removal times

To link leakage magnitude, particle size, and jet transport, two summary measures were defined. The NF emission index at distance $x \in \{1, 2, 3\}$ is

$$NF = TOL \times \frac{v(x)}{v_{ref}(x)} \tag{6}$$

where $v(x)$ is the measured horizontal exhalation velocity at $x = 1, 2, 3$ ft and $v_{ref}(x)$ is a fixed reference (e.g. no-covering, 39 L min^{-1}) so that NF(x)=1 represents the worst observed NF condition. This metric approximates distance-specific source strength. The FF index is

$$FF = TOL \times \frac{1}{\Lambda} \tag{7}$$

linking emission strength (TOL) to the room's total first-order removal rate Λ.

Experimental design and data analysis

We used a factorial design with fixed factors: device type (five levels), flow (17, 28, 39 L min^{-1}), and faceseal (0%, 50%, 100%), plus a no-covering reference. Covered conditions were tested in six independent donnings per type × flow × faceseal combination ($N = 6$) on the same hard headform; the no-covering reference was repeated three times ($N = 3$). Primary analyses used a mixed-effect analysis of variance (ANOVA) model aligned with this design [39]:

$$y_{ijkl} = \mu + \alpha_i + \beta_j + \gamma_k + (\alpha\beta)_{ij} + (\alpha\gamma)_{ik} + \epsilon_{ijkl} \begin{cases} i = 1,2,3,4,5 \\ j = 1,2,3 \\ k = 1,2,3 \\ l = 1,2 \end{cases} \tag{8}$$

where α_i is the effect of device type, β_j is the effect of faceseal, γ_k is the effect of flow rate, $(\alpha\beta)_{ij}$ is the interaction of device type and faceseal, $(\alpha\gamma)_{ik}$ is the interaction of device type and flow rate, and ϵ_{ijkl} is the random error. The statistical analysis was conducted using JMP Pro Software (JMP®, Version 16. SAS Institute Inc., Cary, NC, 1989–2021) to evaluate the main effects of various factors on horizontal velocity. *P*-values $\leq$ 0.05 were considered significant.

Quality assurance

Instrumentation was calibrated according to the manufacturer's recommendations every year. Before each session, background checks of the sampling lines were performed; acceptance criteria were $C_{bg} \leq 500$ particles•cm^{-3}.

Results

Device type was the dominant determinant of both leakage and leaked-aerosol size, whereas breathing flow primarily shifted particle size but not leakage magnitude. In the mixed-effect ANOVA (Table I), device type was significant for TOL ($F = 7.6$, $P = 0.01$) and CMD ($F = 7.1$, $p = 0.01$). Flow rate did not affect TOL ($F = 0.9$, $P = 0.40$) but did affect CMD ($F = 3.8$, $P = 0.03$). Faceseal was not significant as a main effect ($P \geq 0.41$), but the device type × faceseal interaction was significant for both endpoints (TOL: $F = 6.8$, $P < 0.01$; CMD: $F = 2.9$, $P = 0.01$), indicating product-specific sensitivity to faceseal condition. Device type × flow rate was not significant ($P \geq 0.89$), so device rankings were stable across 17, 28, and 39 L min^{-1}.

Figure 3a shows the normalised particle size distribution of leaked aerosols for the no-covering reference with peaks ~1 μm. Figure 3b demonstrates clear size-dependent removal across devices. The non-valved N95 FFR achieved the highest reduction, approaching ≳90% across most bins above ~0.6 μm and remaining high down to ~0.3–0.4 μm. The SM and EHMRSM provided moderate to high reduction (roughly 50–90% over 0.6–6 μm) with a trough near ~3 μm. The N95 FFRV was intermediate between SM/EHMRSM and N95 FFR. The EHMR showed the lowest reduction overall, with a pronounced minimum near ~3 μm.

Table II integrates leakage magnitude (TOL), leaked aerosol size (CMD), and jet momentum (peak centreline velocity at 1, 2, 3 ft). As designed, the no-covering reference performed worst (TOL=100% at all flows), had the largest CMD (0.69–0.72 μm), and produced the fastest jets that strengthened with flow (e.g. v_{1ft}: 39.12–83.48 cm s^{-1}). Among covered devices, EHMR leaked most (82–88%; CMD 0.55–0.61 μm) and retained measurable horizontal velocities, increasing with flow (e.g. v_{1ft}: 42.16–57.07 cm s^{-1}). The FFRV showed intermediate to high TOL rising with flow (38–58%), CMD ~0.45–0.49 μm, and non-zero jets (e.g. v_{1ft}: 21.00–33.77 cm s^{-1}). The SM and EHMRSM strongly attenuated jet momentum despite appreciable leakage (SM: 39–43%; EHMRSM: 73–75%). The non-valved N95 FFR was most protective overall, combining the lowest TOL (5–9%), the smallest CMD among covered devices (~0.42–0.43 μm), and effectively negligible horizontal velocities at all distances. These aggregate rankings align with the size-resolved reduction results and reinforce the predominance of submicron leakage (Figure 3).

Using the leaked aerosol CMD as the representative diameter, we derived slip-corrected particle-scale metrics – τ, v_s , and ACH$_{grav}$ – to evaluate room-scale exposure persistence (Table III). Device type produced a monotonic ordering that was stable across flow rates. Non-valved N95 FFRs yielded the smallest τ (7.41–7.84 $\times 10^{-7}$ s) and v_s (7.27–7.69 $\times 10^{-4}$ cm s^{-1}), corresponding to ACH$_{grav}$ ≈ 0.017–0.018 h^{-1}. Values reported for N95 FFRVs were slightly higher than those for N95 FFRs (τ = 8.41–9.68 $\times 10^{-7}$ s; v_s = 7.27–7.69 $\times 10^{-4}$ cm s^{-1}; ACH$_{grav}$ ≈ 0.020–0.023 h^{-1}). Values reported for SM were intermediate (τ = 8.43–10.47 $\times 10^{-7}$ s; v_s = 8.27–10.28 $\times 10^{-4}$ cm s^{-1}; ACH$_{grav}$ ≈ 0.020–0.025 h^{-1}). The EHMR showed the largest values among covered devices (τ = 12.08–14.70 $\times 10^{-7}$ s; v_s = 11.85–14.42 $\times 10^{-4}$ m s^{-1}; ACH$_{grav}$ ≈ 0.028–0.035 h^{-1}), while EHMRSM shifted these metrics downward toward SM levels (τ = 10.36–11.00 $\times 10^{-7}$ s; v_s = 10.16–11.79 $\times 10^{-4}$ cm s^{-1}; ACH$_{grav}$ ≈ 0.024–0.026 h^{-1}). The no-covering condition generated the largest τ and v_s (τ = 17.72–19.08 $\times 10^{-7}$ s; v_s = 17.39–19.08 $\times 10^{-4}$ cm s^{-1}) and, consequently, the highest gravitational clearance (ACH$_{grav}$ ≈ 0.042–0.046 h^{-1}).

Figure 4 summarises NF emission and FF persistence. The left panel shows the NF index NF at 1, 2, and 3 ft. The EHMR exhibits the largest NF at all distances, indicating substantial jet-driven delivery. The N95 FFRV and SM are an order of magnitude lower, and the non-valved N95 FFR approaches zero, consistent with the suppression of horizontal jets. The EHMRSM also yields very low NF, confirming that masking the EHMR valve collapses jet momentum. The right panel displays the FF index FF evaluated for settling only (ACH$_{grav}$) and for clinical ventilation of 6 and 12 ACH. Across devices, FF tracks source strength: EHMR and EHMRSM are highest, SM and N95 FFRV are intermediate, and N95 FFR is lowest. Increasing ACH from 6 to 12 approximately halves FF for every device, whereas settling alone produces persistence two orders of magnitude longer than with ventilation, underscoring that gravitational deposition contributes little

Table I
ANOVA for TOL and CMD with fixed effects of device type, flow rate, and faceseal

Source	TOL				CMD			
	SS	DF	F	*P*-value	SS	DF	F	*P*-value
Device type	5.3	4	7.6	0.01	238465.0	4	7.1	0.01
Flow rate	0.0	2	0.9	0.40	21603.3	2	3.8	0.03
Faceseal	0.3	2	1.0	0.41	5366.8	2	0.3	0.74
Device type × flow rate	0.1	8	0.4	0.89	9470.9	8	0.4	0.91
Device type × faceseal	1.4	8	6.8	<0.01	67133.0	8	2.9	0.01

ANOVA, analysis of variance; TOL, total outward leakage; CMD, count median diameter; SS, sum of squares; DF, degree of freedom; F, F-statistic.

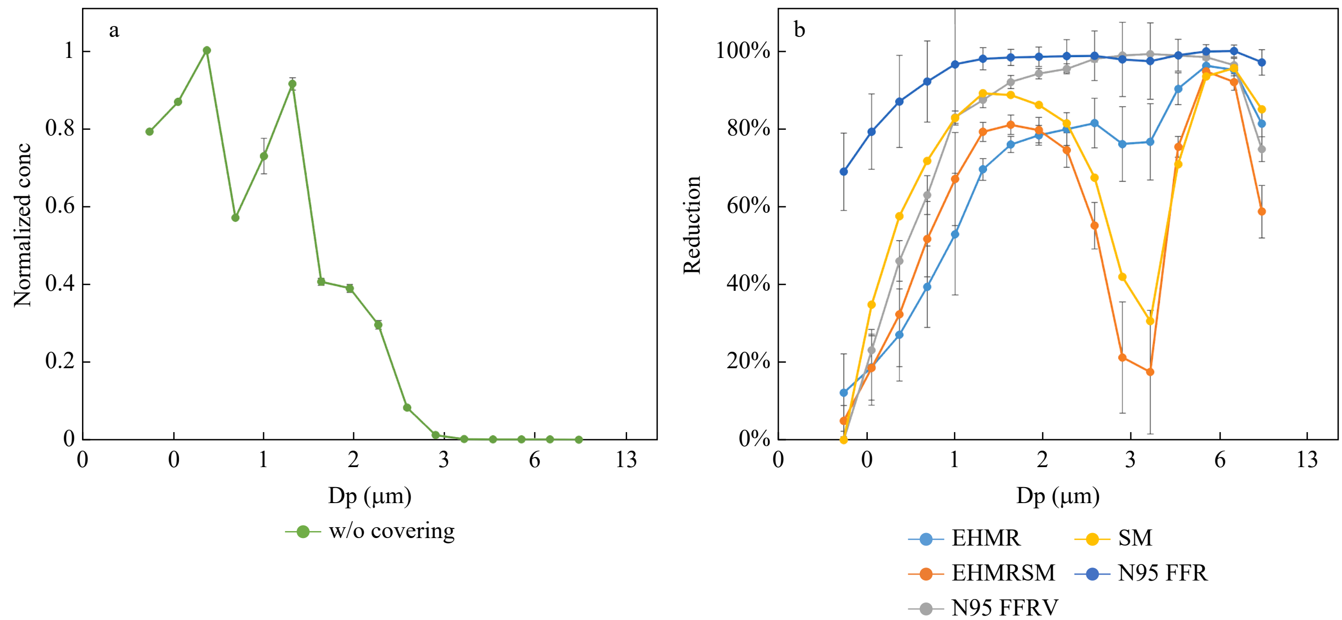

Figure 3. Normalised particle size distribution of leaked aerosols without covering and device-specific removal. Error bars show ± standard error of mean (SEM) across conditions. D_p = mid-point diameter (μm). EHMR, elastomeric half-mask respirator; EHMRSM, EHMR with a surgical mask overlay; N95 FFR, N95 filtering facepiece respirator; N95 FFRV, filtering facepiece respirator valved; SM, surgical mask.

to room-average clearance for these submicron leaks. Together, the panels convey that device choice controls bedside emission (NF) and strongly influences room-average burden (FF), while ventilation determines the timescale of persistence.

Discussion

This study links device-level source control to building-scale exposure by jointly measuring leakage magnitude (TOL), leaked aerosol size (CMD), and horizontal jet momentum (peak

Table II
Summary statistics (mean ± SD) for TOL, CMD, and peak horizontal exhalation velocity at 1, 2, and 3 ft from the headform by device type and breathing flow rate

Device type	Flow rate	*N*	TOL (%)	CMD (μm)	v_{1ft} (cm·s^{-1})	v_{2ft} (cm·s^{-1})	v_{3ft} (cm·s^{-1})
			Mean	Mean	Mean	Mean	Mean
EHMR	17	6	82.30 ± 7.50	0.55 ± 0.11	42.16 ± 10.27	27.26 ± 6.14	18.71 ± 3.82
	28	6	87.67 ± 5.34	0.58 ± 0.11	47.67 ± 8.05	32.34 ± 7.37	22.94 ± 8.97
	39	6	81.97 ± 8.30	0.61 ± 0.09	57.07 ± 15.12	41.40 ± 10.93	31.41 ± 8.15
EHMRSM	17	6	73.82 ± 11.28	0.50 ± 0.07	1.19 ± 0.76	1.19 ± 1.10	1.10 ± 1.04
	28	6	72.94 ± 13.42	0.51 ± 0.04	1.10 ± 0.68	1.52 ± 1.20	0.34 ± 0.26
	39	6	75.20 ± 14.34	0.52 ± 0.05	0.85 ± 0.41	1.19 ± 0.76	0.76 ± 0.62
N95 FFR	17	6	10.68 ± 9.46	0.42 ± 0.03	0.76 ± 0.28	0.34 ± 0.41	0.42 ± 0.21
	28	6	5.45 ± 9.20	0.43 ± 0.03	1.02 ± 0.56	0.17 ± 0.26	0.42 ± 0.38
	39	6	8.30 ± 11.12	0.43 ± 0.03	0.76 ± 0.28	0.34 ± 0.41	0.34 ± 0.41
N95 FFRV	17	6	38.26 ± 17.61	0.45 ± 0.02	21.00 ± 4.00	13.04 ± 5.73	7.03 ± 3.81
	28	6	48.51 ± 20.44	0.47 ± 0.01	26.92 ± 4.25	20.40 ± 4.07	12.28 ± 5.75
	39	6	58.14 ± 21.95	0.49 ± 0.02	32.77 ± 8.27	22.86 ± 6.43	15.66 ± 6.05
SM	17	6	39.39 ± 30.66	0.45 ± 0.04	1.19 ± 0.69	1.44 ± 1.38	0.42 ± 0.38
	28	6	41.06 ± 30.44	0.51 ± 0.06	2.03 ± 1.73	0.76 ± 0.43	0.59 ± 0.38
	39	6	43.07 ± 28.34	0.49 ± 0.06	2.20 ± 1.72	1.10 ± 0.68	0.42 ± 0.21
No covering	17	3	100.00 ± 0.00	0.69 ± 0.01	39.12 ± 5.66	26.75 ± 2.05	16.76 ± 0.51
	28	3	100.00 ± 0.00	0.71 ± 0.01	54.53 ± 2.56	34.37 ± 1.28	26.59 ± 1.47
	39	3	100.00 ± 0.00	0.72 ± 0.01	83.48 ± 5.01	46.40 ± 1.55	33.87 ± 0.59

v_{1ft}, v_{2ft}, and v_{3ft} are the peak centreline velocities at 1, 2, 3 ft, respectively.
SD, standard deviation; TOL, total outward leakage; CMD, count median diameter; EHMR, elastomeric half-mask respirator; EHMRSM, EHMR with a surgical mask overlay; N95 FFR, N95 filtering facepiece respirator; N95 FFRV, N95 filtering facepiece respirator valved; SM, surgical mask

Table III
CMD-derived aerosol dynamics and gravitational clearance metrics (mean ± SD) by device type and flow

Device type	Flow rate	N	τ ($\times 10^{-7}$ s)	v_s ($\times 10^{-4}$ cm s^{-1})	ACH_{grav} (h^{-1})
EHMR	17	6	12.075 ± 4.579	11.846 ± 4.492	0.028 ± 0.011
	28	6	13.517 ± 4.638	13.260 ± 4.550	0.032 ± 0.011
	39	6	14.701 ± 4.068	14.422 ± 3.991	0.035 ± 0.010
EHMRSM	17	6	10.357 ± 2.690	10.160 ± 2.638	0.024 ± 0.006
	28	6	10.575 ± 1.548	10.374 ± 1.519	0.025 ± 0.004
	39	6	11.000 ± 1.718	10.789 ± 1.685	0.026 ± 0.004
N95 FFRV	17	6	8.410 ± 0.596	7.269 ± 0.766	0.020 ± 0.001
	28	6	9.041 ± 0.500	7.624 ± 0.825	0.021 ± 0.001
	39	6	9.678 ± 0.645	7.687 ± 0.869	0.023 ± 0.002
N95 FFR	17	6	7.410 ± 0.781	7.269 ± 0.766	0.017 ± 0.002
	28	6	7.771 ± 0.841	7.624 ± 0.825	0.018 ± 0.002
	39	6	7.836 ± 0.886	7.687 ± 0.869	0.018 ± 0.002
SM	17	6	8.434 ± 1.223	8.274 ± 1.200	0.020 ± 0.003
	28	6	10.475 ± 2.151	10.276 ± 2.110	0.025 ± 0.005
	39	6	9.951 ± 1.950	9.762 ± 1.913	0.023 ± 0.005
No covering	17	3	17.722 ± 0.280	17.386 ± 0.275	0.042 ± 0.001
	28	3	18.847 ± 0.464	18.489 ± 0.455	0.044 ± 0.001
	39	3	19.446 ± 0.419	19.076 ± 0.411	0.046 ± 0.001

Note: τ is Stokes relaxation time; v_s is the terminal settling velocity; ACH_{grav} is gravitational deposition.
CMD, count median diameter; SD, standard deviation; ACH, air changes per hour; EHMR, elastomeric half-mask respirator; EHMRSM, EHMR with a surgical mask overlay; N95 FFR, N95 filtering facepiece respirator; N95 FFRV, filtering facepiece respirator valved; SM, surgical mask.

centreline velocity) and by embedding those measurements in a first-order removal framework relevant to healthcare rooms. Device type was the primary determinant of source control: non-valved N95 FFRs minimised both TOL and NF jet transport; N95 FFRVs were intermediate; EHMRs showed the largest outward leakage. The SMs and EHMRSM collapsed horizontal jets to near the detection limit but still permitted appreciable leakage. These patterns were robust across 17–39 L min^{-1} and align with the mechanism: filtration efficiency, faceseal performance, and the presence/absence of an unfiltered exhalation path jointly govern outward emission. Our NF and FF indices make these trade-offs explicit by separating jet-driven delivery at 1–3 ft from room-average persistence.

The superior source control of non-valved N95 FFRs agrees with manikin and simulator studies showing higher collection efficiencies than surgical or cloth masks [40]. Guidance on valved respirators cautions against unfiltered outward flow and recommends either non-valved devices for source control or valve overlays when valved models must be used [21,23]. Our data — high TOL for EHMRs and intermediate TOL for

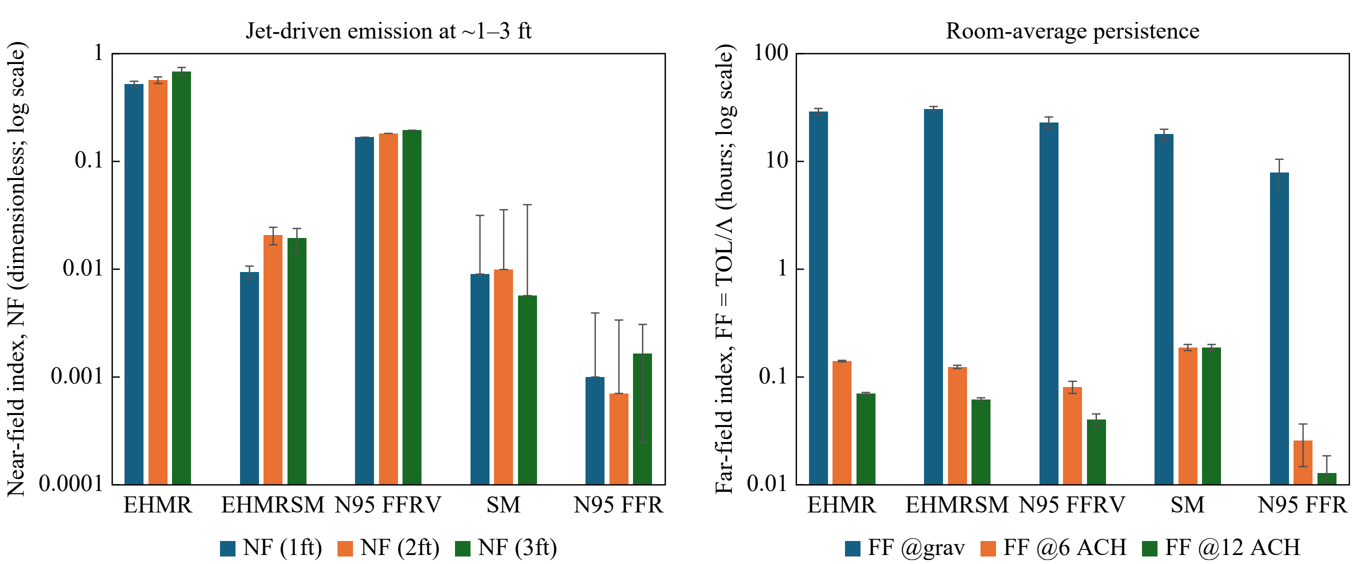

Figure 4. Room-average persistence by device type, expressed as the far-field index FF at clinical ventilation (Λ = 6 and 12 ACH) and for gravitational settling alone (ACH_{grav}). ACH, air changes per hour; EHMR, elastomeric half-mask respirator; EHMRSM, EHMR with a surgical mask overlay; FF, far-field; N95 FFR, N95 filtering facepiece respirator; N95 FFRV, filtering facepiece respirator valved; NF, near-field; SM, surgical mask; TOL, total outward leakage.

FFRVs – are consistent with that caution, while acknowledging that specific valved designs can outperform loose face coverings. The emergence of EHMRs with filtered valves provides a route to reconcile reusability with source control needs [41].

Visualisations and fluid mechanics work have shown repeatedly that masks attenuate or redirect exhalation jets. Our near-zero horizontal velocities for SM, EHMRSM, and non-valved N95s at 1–3 ft agree with these observations, whereas measurable jets for EHMRs and FFRVs are consistent with an open exhalation path [28]. Across device types, leaked aerosols were overwhelmingly submicron (peaking ~0.35–0.40 μm) and notably smaller than emissions without source control (bimodal peaks near 0.50 and 1.00 μm), in line with classic exhalation modes and hospital air studies that size viral RNA [42–44].

Using CMD-derived, slip-corrected settling velocity, we found gravitational loss rates of ~0.02–0.05 h^{-1} – negligible compared with clinical ventilation and filtration – so FF concentrations are governed by the total removal rate Λ, dominated by clean-air delivery rather than deposition. This agrees with well-mixed mass-balance formulations in which emissions set steady-state burden and removal sets clearance time [11].

Embedding TOL in a first-order model translates device performance to room scale: for a given ACH, lower TOL directly lowers steady-state concentration and integrated dose. The FF index formalises this linkage; the NF index (TOL scaled by jet velocity at distance) targets the 1–3 ft zone where momentum dominates. This NF/FF separation mirrors risk frameworks used in indoor transmission modelling and operational guidance [11].

Practically, in rooms with 6–12 ACH or higher, the principal lever on FF burden is source strength (leakage). On this dimension, non-valved N95 FFRs are preferable to SMs, FFRVs, and EHMRs; EHMRs without filtered/covered valves should be avoided when source control is required. At the near field, devices that both leak more and maintain stronger jets (EHMRs, some FFRVs) pose greater short-range risk, whereas SM overlays on EHMRs markedly reduce NF even if TOL remains high. Although N95 FFRVs showed TOL comparable with SM, the SM substantially reduced exhalation-jet momentum at the near field, yielding a low NF. These observations cohere with guidance discouraging unfiltered valves and with demonstrations that masks reduce jet reach and dispersion [21,45].

Relative to prior TOL-centric reports, our work adds two advances. First, we pair size-resolved leakage with direct jet-velocity measurements, linking 'how much' to 'how it travels' at clinically relevant distances. Second, we embed both in a ventilation-aware framework to yield practical NF and FF indices that can be read directly against room ventilation ACH and filtration – providing a bridge from bench measurements to building operation [11,30].

Limitations include use of a single medium-sized hard-surface headform, which cannot represent facial variability, speech/motion, or microclimate effects; chamber testing with NaCl and OPS sizing over 0.30–10 μm (excluding ultrafine particles that would, if anything, further diminish the role of settling); and characterisation of horizontal jet momentum without full 3D plume evolution in a ventilated room. Future work should incorporate diverse headforms and human subjects, speech/cough flows, and coupled manikin–CFD/zonal modelling at clinical ACH to refine NF/FF guidance.

In US practice, using an EHMR with an external surgical-mask overlay constitutes a configuration outside the original National Institute for Occupational Safety and Health (NIOSH) approval unless specifically authorised by the manufacturer. Accordingly, our EHMR with SM overlay findings should be interpreted as experimental performance data rather than a deployment recommendation; programmes requiring source control should preferentially use non-valved EHMRs or manufacturer-approved filtered valve models and follow institutional policies. Future work will extend this framework to EHMRs with filtered exhalation valves and valveless EHMRs, quantifying size-resolved outward leakage, jet suppression, and room-scale persistence alongside physiological and usability endpoints (e.g. exhalation resistance/work of breathing) and addressing regulatory implications for clinical deployment.

In conclusion, this study quantified three device-level source terms – TOL, CMD, and exhalation-jet momentum – and translated them to building scale using two operational metrics: an NF index for jet-driven transport at 1–3 ft and an FF index that links leakage to room persistence via Λ. Device type dominated emission strength: non-valved N95 FFRs minimised leakage and jet momentum (negligible NF; lowest FF); EHMRs with unfiltered valves produced the highest emissions and persistent jets (highest NF and FF); SMs and EHMRSMs collapsed jets (low NF) but retained moderate to high leakage, sustaining elevated FF unless Λ is increased.

Leaked aerosols were overwhelmingly submicron (CMD ~0.42–0.61 μm), making gravitational settling a minor contributor to Λ compared with ventilation and filtration typical of healthcare rooms. In practice, device choice sets the source, and Λ – delivered by outdoor air, recirculated filtration, and portable or central air cleaning – sets the persistence timescale. Effective control therefore pairs low-leakage devices (preferably non-valved N95s for source control, or valved devices with filtered/covered exhalation) with adequate equivalent clean air (e.g. 6–12 ACH for patient care), rather than relying on deposition. The NF/FF framework makes these decisions actionable: NF highlights residual short-range risk unless both leakage and jet momentum are reduced; FF supports back-calculating clean-air delivery to meet steady-state or clearance targets for a given device mix. These findings support performance-based design, retrofit, and operation of healthcare spaces and provide a transparent bridge from bench measurements to environmental-hygiene practice.

CRediT authorship contribution statement

W. Yang: Writing – original draft, Visualization, Validation, Software, Methodology, Investigation, Data curation, Conceptualization. **W.R. Myers:** Writing – review & editing, Supervision, Resources, Project administration, Funding acquisition, Conceptualization. **K.J. Ryan:** Writing – review & editing, Validation, Methodology. **L. Zheng:** Writing – review & editing, Validation. **Y. Zhang:** Writing – review & editing, Validation. **X. Li:** Writing – review & editing, Validation.

Ethics statement

This study used headform and laboratory-generated neutralised NaCl aerosols. No human participants, animals, identifiable patient data, or clinical/biological specimens were involved; therefore, institutional ethics approval and informed consent were not required.

Funding sources

This work was funded by the National Institute for Occupational Safety and Health (NIOSH), National Personal Protective Technology Laboratory (NPPTL) (grant number: 75D30120P09521).

Conflict of interest statement

The authors declare that there is no conflict of interest.

Acknowledgements

During the preparation of this work, the authors used ChatGPT in order to improve the grammar and language clarity. After using this tool, the authors reviewed and edited the content as needed and take full responsibility for the content of the publication.

Appendix A. Supplementary data

Supplementary data to this article can be found online at https://doi.org/10.1016/j.jhin.2026.01.024.

References

[1] Greenhalgh T, Jimenez JL, Prather KA, Tufekci Z, Fisman D, Schooley R. Ten scientific reasons in support of airborne transmission of SARS-CoV-2. The Lancet 2021;397:1603–5.
[2] Prather KA, Marr LC, Schooley RT, McDiarmid MA, Wilson ME, Milton DK. Airborne transmission of SARS-CoV-2. Science 2020;370:303–4.
[3] Shelton-Davenport M, Pavlin J, Saunders J, Staudt A, editors. Airborne Transmission of SARS-CoV-2: Proceedings of a Workshopâ€"in Brief. Washington, D.C.: National Academies Press; 2020. https://doi.org/10.17226/25958.
[4] Tay GTP, Niazi S, He C, Morawska L, Bell SC, Spann K, et al. Viable viruses in airborne particles detected during cough by participants with acute respiratory viral infections. J Hosp Inf 2025;164:18–26.
[5] Liu Y, Ning Z, Chen Y, Guo M, Liu Y, Gali NK, et al. Aerodynamic Characteristics and RNA Concentration of SARS-CoV-2 Aerosol in Wuhan Hospitals during COVID-19 Outbreak 2020:2020.03.08.982637. https://doi.org/10.1101/2020.03.08.982637.
[6] Wang CC, Prather KA, Sznitman J, Jimenez JL, Lakdawala SS, Tufekci Z, et al. Airborne transmission of respiratory viruses. Science 2021;373:eabd9149.
[7] Morawska L, Johnson GR, Ristovski ZD, Hargreaves M, Mengersen K, Corbett S, et al. Size distribution and sites of origin of droplets expelled from the human respiratory tract during expiratory activities. J Aer Sci 2009;40:256–69.
[8] Fennelly KP. Particle sizes of infectious aerosols: implications for infection control. Lan Resp Med 2020;8:914–24.
[9] Groma V, Kugler S, Farkas Á, Füri P, Madas B, Nagy A, et al. Size distribution and relationship of airborne SARS-CoV-2 RNA to indoor aerosol in hospital ward environments. Sci Rep 2023;13:3566.
[10] ASHRAE. ASHRAE positions on infectious aerosols 2022.
[11] Bazant MZ, Bush JWM. A guideline to limit indoor airborne transmission of COVID-19. Proc Nat Acad Sci 2021;118:e2018995118.
[12] Bourouiba L. Turbulent gas clouds and respiratory pathogen emissions: potential implications for reducing transmission of COVID-19. JAMA 2020. https://doi.org/10.1001/jama.2020.4756.
[13] Abkarian M, Mendez S, Xue N, Yang F, Stone HA. Speech can produce jet-like transport relevant to asymptomatic spreading of virus. Proc Nat Acad Sci 2020;117:25237–45.
[14] Mittal R, Ni R, Seo J-H. The flow physics of COVID-19. J Fluid Mech 2020;894. https://doi.org/10.1017/jfm.2020.330.
[15] Riley EC, Murphy G, Riley RL. Airborne spread of measles in a suburban elementary school. Am J Epidemiol 1978;107:421–32.
[16] Gammaitoni L, Nucci MC. Using a mathematical model to evaluate the efficacy of TB control measures. Emerg Infect Dis 1997;3:335–42.
[17] Word Health Organization. Roadmap to improve and ensure good indoor ventilation in the context of COVID-19 2021. Available at: https://www.who.int/publications/i/item/9789240021280?utm_source=chatgpt.com [last accessed September 23, 2025].
[18] CDC. Guidelines for environmental infection control in health-care facilities 2003.
[19] Christy L. Operating room HVAC setback strategies | ASHE 2011. Available at: https://www.ashe.org/management_monographs/mg2011love [last accessed September 23, 2025].
[20] CDC. Preventing transmission of viral respiratory pathogens in healthcare settings. Inf Cont 2025. Available at: https://www.cdc.gov/infection-control/hcp/viral-respiratory-prevention/index.html [last accessed September 24, 2025].
[21] CDC. Respiratory protection vs. Source control – what's the difference? | blogs. CDC; 2020. Available at: https://blogs.cdc.gov/niosh-science-blog/2020/09/08/source-control/ [accessed June 20, 2025].
[22] Knobloch JK, Franke G, Knobloch MJ, Knobling B, Kampf G. Overview of tight fit and infection prevention benefits of respirators (filtering face pieces). J Hosp Inf 2023;134:89–96.
[23] NIOSH [2020]. Filtering facepiece respirators with an exhalation valve: measurements of filtration efficiency to evaluate their potential for source control. By Portnoff L, Schall J, Brannen J, Suhon N, Strickland K, Meyers J. U.S. Department of Health and human Services, Centers for Disease Control and Prevention, National Institute for Occupational Safety and Health, DHHS (NIOSH) Publication No. 2021-107.
[24] NIOSH [2022]. Evaluation of exhalation resistance and inspired carbon dioxide concentration in elastomeric half-mask respirators with modified or covered exhalation valves. By Strickland KT, Fernando R, Schall J, Walbert G, Brannen J. U.S. Department of Health and Human Services, Centers for Disease Control and Prevention, National Institute for Occupational Safety and Health, DHHS (NIOSH) Publication No. 2022-109. https://doi.org/10.26616/NIOSHPUB2022109.
[25] Anfinrud P, Stadnytskyi V, Bax CE, Bax A. Visualizing Speech-Generated Oral Fluid Droplets with Laser Light Scattering. New England J Med 2020;382:2061–3.
[26] Blachere FM, Lemons AR, Coyle JP, Derk RC, Lindsley WG, Beezhold DH, et al. Face mask fit modifications that improve source control performance. Am J Inf Control 2022;50:133–40.
[27] Hao W, Parasch A, Williams S, Li J, Ma H, Burken J, et al. Filtration performances of non-medical materials as candidates for manufacturing facemasks and respirators. Int J Hyg Environ Health 2020;229:113582.
[28] Verma S, Dhanak M, Frankenfield J. Visualizing the effectiveness of face masks in obstructing respiratory jets. Phy Fluids 2020;32:061708.
[29] Lindsley WG, Blachere FM, Beezhold DH, Law BF, Derk RC, Hettick JM, et al. A comparison of performance metrics for cloth face masks as source control devices for simulated cough and

exhalation aerosols. medRxiv 2021. https://doi.org/10.1101/2021.02.16.21251850. 2021.02.16.21251850.

[30] Myers WR, Yang W, Ryan KJ, Bergman MS, Fisher E, Soo J-C, et al. Total outward leakage of half-mask respirators and surgical masks used for source control. J Occup Environ Hyg 2023;20:610–20.

[31] Rao L, Lu J, Wang S, Li H, Han W. Evaluating the efficacy of action-based instructions on the suitability of medical protective masks in healthcare settings. J Hosp Inf 2025. https://doi.org/10.1016/j.jhin.2025.10.001. 0.

[32] Greenawald LA, Haas EJ, D'Alessandro MM. Elastomeric half mask respirators: an alternative to disposable respirators and a solution to shortages during public health emergencies. J Int Soc Respir Prot 2021;38:74–91.

[33] CDC. Advancements in elastomeric respirator Technology for use as source control | Blogs. CDC; 2021. Available at: https://blogs.cdc.gov/niosh-science-blog/2021/03/01/elastomeric_source-control/. [Accessed 24 September 2025].

[34] Zhuang E, Thurman P, Chen HH, McDiarmid MA, Hines SE. Physiological Impacts of Surgical Mask Coverage of Elastomeric Half-mask Respirator Exhalation Valves in Healthcare Workers. Ann Work Expo Health 2021. https://doi.org/10.1093/annweh/wxab069. wxab069.

[35] Zhang C, Nielsen PV, Liu L, Sigmer ET, Mikkelsen SG, Jensen RL. The source control effect of personal protection equipment and physical barrier on short-range airborne transmission. Build Environ 2022;211:108751.

[36] Nazaroff WW. Indoor particle dynamics. Indoor Air 2004;14:175–83.

[37] International Organization for Standardization. Respiratory protective devices - human factors - Part 1: metabolic rates and respiratory flow rates 2015.

[38] Zhu J, He X, Bergman MS, Guffey S, Nimbarte AD, Zhuang Z. A pilot study of minimum operational flow for loose-fitting powered air-purifying respirators used in healthcare cleaning services. J Occup Environ Hyg 2019;16:440–5.

[39] Montgomery DC. Design and analysis of experiments. John Wiley & Sons; 2017.

[40] Lindsley WG, Blachere FM, Derk RC, Boots T, Duling MG, Boutin B, et al. Constant vs. cyclic flow when testing face masks and respirators as source control devices for simulated respiratory aerosols. Aer Sci Tech 2023;57:215–32.

[41] Safety+Health. NIOSH approves first elastomeric half-mask respirator without an exhalation valve | 2020-12-01 | Safety+Health. 2020. Available at: https://www.safetyandhealthmagazine.com/articles/20577-niosh-approves-first-elastomeric-half-mask-respirator-without-an-exhalation-valve [last accessed September 28, 2025].

[42] Morawska L, Buonanno G, Mikszewski A, Stabile L. The physics of respiratory particle generation, fate in the air, and inhalation. Nat Rev Phys 2022;4:723–34.

[43] Lai J, Coleman KK, Tai S-HS, German J, Hong F, Albert B, et al. Relative efficacy of masks and respirators as source control for viral aerosol shedding from people infected with SARS-CoV-2: a controlled human exhaled breath aerosol experimental study. eBioMedicine 2024;104. https://doi.org/10.1016/j.ebiom.2024.105157.

[44] Tang S, Mao Y, Jones RM, Tan Q, Ji JS, Li N, et al. Aerosol transmission of SARS-CoV-2? Evidence, prevention and control. Environ Int 2020;144:106039.

[45] CDC. Strategies for Conserving the Supply of N95® Filtering Facepiece Respirators. Healthcare Workers 2025. https://www.cdc.gov/niosh/healthcare/hcp/pandemic/conserving-n95.html [last accessed September 23, 2025].